Comparative study on the aerodynamic performance of airfoil with boundary layer trip of various geometrical shapes

Comparative study on the aerodynamic performance of airfoil with boundary layer trip of various geometrical shapes

Sreejith B. K.[*], **Sathyabhama A.**[a] **and Sandeep Kumar S.**[b]

[*] AJ Institute of Engineering and Technology, Mangaluru, Karnataka, India-575006
[a,b]National Institute of Technology Karnataka, Mangaluru, Karnataka, India-575025

E-mail: srijithbk@gmail.com[*], bhama72@gmail.com[a] and sksandeep575@gmail.com[b]

Abstract. Performance of small scale wind turbine (SSWT) and miniature aerial vehicles (MAV) is always effected with Laminar separation bubble. The problem of a laminar separation bubble on the upper surface of an E216 airfoil operated at low Reynolds number (Re=100000) is investigated numerically. Incompressible steady two-dimensional simulation is carried out with Transition $\gamma - Re_\theta$ turbulence model on the airfoil with a boundary layer trip (BLT). The performance of two different types of trips, namely, isosceles triangular (IT) and right-angled triangular (RA) is compared with that of the airfoil with a rectangular (RT) trip. The trip locations used are, 17% of the chord for location-1 and 10% of the chord for location-2 from the leading edge of the airfoil, while the trip heights selected are 0.3 mm, 0.5 mm, 0.7 mm, and 1 mm. Results showed that the boundary layer trip significantly affected the laminar separation and improved the aerodynamic performance of the airfoil. Maximum improvement in drag by 17.41% and corresponding lift to drag ratio by 10.86% are obtained for the isosceles trip at location-2 for the angle of attack of 6°. There is no observable advantage for isosceles and right-angled triangular trips over rectangular trips. Considering the geometrical complexity in fabrication, the rectangular trip is recommended.

Key words: Airfoil, Boundary layer trips, Laminar flow, Laminar separation bubbles, Small scale wind turbine.

List of symbols

c	Chord length,m
C_p	Coefficient of pressure
C_d	Drag coefficient
C_l	Lift coefficient
k	Turbulent kinetic energy, m^2/s^2
Re	Reynold number based on chord length
Re_θ	Momentum thicknes Reynold number b
x/c	Axial distance over airfoil along axial chord

Greek symbols

α	Angle of attack, ^{0}
γ	intermittency

Abbreviations

AOA	Angle of attack

CFD	Computational fluid dynamics
IT	Isosceles triangular
LSB	Laminar separation bubble
2D	Two dimensional
R	Reattachment point
RA	Right-angled triangular
RT	Rectangular
SIMPLE	Semi-implicit method for pressure-linked equations
SSWT	Small scale wind turbines
RANS	Reynolds averaged Navier–Stokes
TKE	Turbulent kinetic energy

1. Introduction

Wind energy is an efficient renewable power source and is an alternate energy resource to replace fossil fuel in the present and future. The development in the field of small and micro wind turbine systems has made it possible to generate energy even in the regions of low wind speed and in urban areas. The small scale wind turbines (SSWTs) can be used even in remote locations as independent or as microgrid feeders where electricity from conventional power resources are not feasible [1, 2]. The systems with rotor swept area $\leq 200m^2$ with generated power $\leq 50kW$ [3] are classified as SSWTs. The poor wind resource in the site and small swept area of the SSWT, make it to work under low Reynolds number ($Re \leq 10^5$) [4, 5] condition. The Laminar separation bubble (LSB) formation is a common aerodynamic phenomenon observed on the SSWT blades in such low Re environment [6]. During low Reoperation, the low energy laminar flow over the blade may not withstand the adverse pressure gradient (APG). Consequently, the flow separates from the blade surface promoting reversed flow with mixing and momentum exchange with adjacent flow field. Finally, the flow converts to turbulent and regains sufficient energy and continues as attached flow [7]. The region between the flow separation and reattachment where a recirculating dead air zone is formed is termed as LSB [8].

The stream-wise momentum equation inside the boundary layer is approximated as,

$$u\frac{\partial u}{\partial x} = -\frac{1}{\rho}\frac{\partial p}{\partial x} = \nu\frac{\partial^2 u}{\partial y^2} \tag{1}$$

APG occurs when $\frac{\partial p}{\partial x} > 0$, which causes the velocity u to decrease along x and the velocity becomes zero if the APG is strong enough. At this point of operation, a slow reversal occurs and flow separates from airfoil surface. Skin friction coefficient (C_f) has a great influence on LSB formation. Von Karman integral boundary-layer equation [9] can be written as,

$$\frac{1}{\rho u_e^2\theta}\frac{d(\rho u_e^2\theta)}{d(\xi)} = \frac{C_f}{2\theta} - \frac{H}{u_e}\frac{du_e}{d\xi} \tag{2}$$

where ξ is the boundary-layer co-ordinate, u_e is the boundary-layer edge velocity. The term H is shape factor, defined as the ratio between the boundary-layer momentum thickness (θ) and the boundary-layer displacement thickness (δ^*).

The skin friction inside the bubble is nearly zero [10] and then Eq. 2 becomes,

$$\frac{\Delta(\rho u_e^2\theta)}{\rho u_e^2\theta} \simeq -H\frac{\Delta u_e}{u_e} \tag{3}$$

and can be re-writen as,

$$\Delta(\rho u_e^2 \theta) \simeq \rho u_e \delta^* \Delta u_e \tag{4}$$

It can be observed that the increase in drag $\Delta(\rho u_e^2 \theta)$ due to LSB is proportional to the product of average mass defect $\rho u_e \delta^*$ and edge velocity jump Δu_e. It implies that the size and position of the LSB are the functions of the airfoil shape, AOA, Re and environmental conditions [11].

The main effect of LSB is an increase in boundary layer thickness which increases pressure drag due to pseudo thickness of airfoil and loss in lift [12]. By controlling the LSB formation, wind turbine blade performance can be improved. The premature transition of the laminar boundary layer into a turbulent boundary layer using any external means (such as flow control techniques) is the most effective method of LSB elimination [13]. Passive and active vortex generation methods are being developed and are proved to be successful in reducing the effects of the LSB over the low Re airfoils [14]. Boundary layer grits, boundary layer wires, boundary layer trips (BLT) and surface dimples are some of the passive flow control techniques used to control LSB. They are simple and comparatively the most acceptable methods for wind turbine application than active flow control methods. Use of mechanical BLT like trip wires, plain trips, zigzag tape, etc is the most effective methods of LSB elimination currently in use. Many studies have been carried out to find the performance and effectiveness of BLT on various airfoils at different flow conditions. Mccrossen et al. [15] studied the effect of BLT located at various chord-wise locations on Clark Y12 airfoil at Re between 62,000 and 209,000. They reported a significant increase in drag than the lift for the airfoil with BLT at higher Re. The BLT improved the performance in the low Re range up to 135,000 only. Bai et al. [16] and Gopalarathnam et al. [17] also observed similar performance of BLT. Jones et al. [18] experimented in low Re range 40,000 $\leq Re \leq$ 120,000 on E423 airfoil, and found that the tape trips improved the lift at low AOA and higher Re range and reduced the drag at low Re. Improved drag and the reduced lift is reported for most of the cases by Traub et al. [19]. It proves that the BLT performance depends on the type of airfoil and the net advantage depends on the relative benefit between lift and drag coefficients and hence effect on C_l/C_d ratio should be studied as a performance parameter. BLT works better when the flow transition completes before the boundary layer reattachment point [20]. Complex trip geometries such as 3-D, zigzag etc and multiple trips produced little benefit over single 2-D plain trips [21]. Effective drag reduction requires thin BLT. The 2D trips are more acceptable because of its simple structure and easy fabrication. Hence, a detailed study on the plain 2D trip of different shapes namely, isosceles triangular (IT) and right-angled triangular (RA) is carried out in this paper. Two-dimensional numerical simulation is carried out to study the aerodynamic performance and the flow structure on airfoil E216 with IT and RA BLTs for $4°, 6°$ and $8°$ AOA and at Re of 100,000 using Menter's $\gamma - Re_\theta$ transition model. . Performance evaluation is done for two chord-wise locations of the trip, 17% of chord for location-1 and 10% of chord for location-2 from the leading edge of the airfoil and trip heights of 0.3 mm, 0.5 mm, 0.7 mm, and 1mm. The results are compared with the author's published results [22] for baseline and airfoil with rectangular (RT) trip to ascertain whether the geometry of the trip has any effect on the LSB.

Highly developed modern CFD methods can be used to model turbulent and transitional flow effectively and accurately with improved computational power [23, 24]. The expensive experimental methodology can be replaced with such CFD studies. Numerical simulation can provide a deep understanding of the flow physics and aerodynamic behaviour of the airfoil. Reynolds Averaged Navier-Stokes (RANS) methods are accurate and well-validated CFD simulation tool for analysing complex flow phenomena. However, the popular RANS turbulent models such as $k - \omega$, $k - \varepsilon$, etc assume a fully turbulent regime in the entire flow field and fail to predict the boundary transition phenomena such as LSB [25] due to airfoil's thick boundary

layers and complicated viscous effects at low Re due to the presence of LSB [19]. Though large eddy simulation (LES) and direct numerical simulations (DNS) are good in such cases, these methods are computationally demanding and require long calculation time [26, 27, 28]. Intermittency (γ) concept introduced by Dhawan et al. [29] to predict transition and its further development by Menter et al. [30] made it possible to use RANS model for phenomenon such as LSB formation. This model is reported to have a distinct advantage of associating transition modelling with experimental data [31, 32, 33, 34] and the same turbulence model is used in the present study.

2. Methodology

The airfoil E216 selected for the study, is a cambered low Re airfoil suitable for SSWT [22]. A 2D view of the airfoil is shown in figure 1. It is a thin airfoil with maximum thickness of 10.4% at $x/c = 26.2\%$ and camber of 4.7% at $x/c = 59\%$.

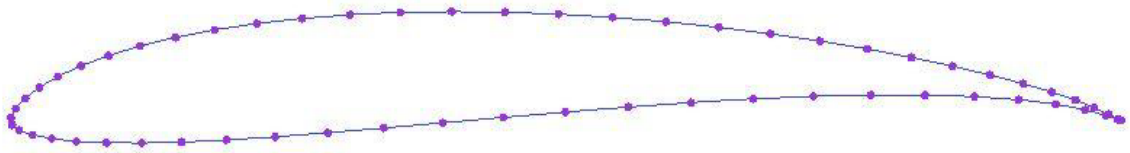

Figure 1: E216 airfoil profile [22]

2.1. Computational method

The computational approach adopted for the study is the same as that presented in our previous published paper of the same authors [22]. The grid configuration used is also the same. The ICEM-CFD is used to create geometry and mesh. The trip geometries are shown in figure 2. A C-type computational domain with a structured grid is used and is shown in figure 3. The computational domain has a length of 9c in front of the airfoil to achieve fully developed flow and 15c behind the airfoil where c is the chord length. The width is 20 times the chord. Fine mesh is created close to the airfoil where the study is mainly focused as shown in figure 4. The mesh adjacent to the surface is set in such a way that it results in y+ value less than one to capture boundary layer phenomena. No-slip condition is used on the airfoil with the velocity at the inlet section. The wall boundary condition is selected at top and bottom boundaries and pressure outlet at the exit of the flow domain. Simulation is carried out at a fluid temperature of 308 K. Free stream inlet velocity of air is set to 10.08 m/s which corresponds to Re of 100,000 and airfoil chord length of 0.15 m. Flow is considered as steady and incompressible. The semi-implicit method for pressure linked equations (SIMPLE) algorithm [33] and second-order upwind spacial discretization is used in the methodology to solve the momentum equations. Least square cell-based spacial gradient scheme is used. Convergence criterion of 10^{-6} is set residuals.

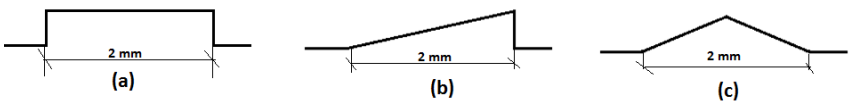

Figure 2: Different shapes of BLT used in the study: (a) rectangle, (b) right-angled triangle, (c) isosceles triangle

Table 1: Grid number used for different kind of BLT model

Model	Number of elements
RT	535,000
RA	507,000
IT	512,000

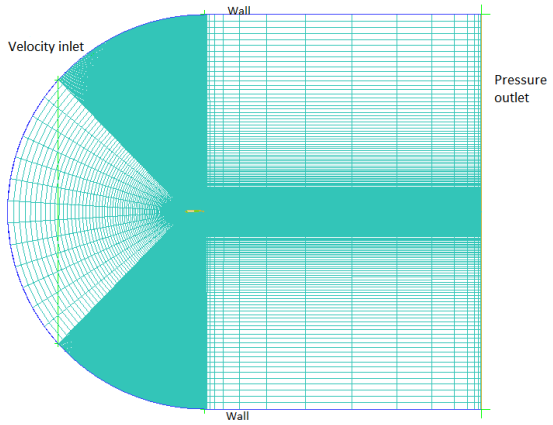

Figure 3: Far view of structured grid in the domain with boundary conditions [22]

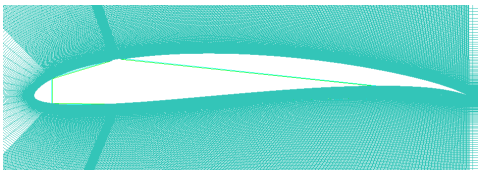

Figure 4: Close view of dense grid around the airfoil [22]

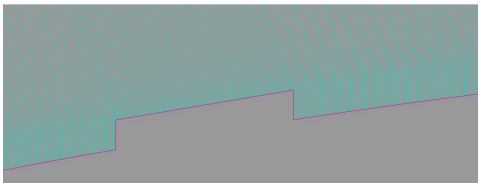

Figure 5: Grid configuration near the BLT [22]

2.2. Turbulence model

The performance of airfoils and modelling of LSB is carried out using Langtry-Menter 4-equation Transitional SST Model or $\gamma - Re_\theta$ - SST [31]. It is based on the two-equation $k-\omega$ SST model with one for intermittency (γ)and another for transitional Reynolds number ($Re_{\theta t}$) equations to capture the laminar-turbulent transition process. The production term in the turbulent kinetic energy (TKE) is activated using γ term after the transition point and the $Re_{\theta t}$ term used to model the non-local effect of the turbulence intensity (TI) [31].

Grid independence test is conducted with five sets of meshes ranging from 10,000 to 610,000 elements for baseline, RT, RA and IT BLTs of 1mm trip height. Then same pattern mesh is used for respective trip shapes with all other trip heights. The C_l and C_d are the parameters checked for the grid consistency. The simulations are carried out for AOA of 6^0 and the results for the baseline test are shown in figure 6. After around 475,000 grid cells there is no significant variation in lift coefficient and hence it is considered as appropriate mesh size for further simulations for the baseline model. A similar procedure is followed for modified models and the Table 1 gives the final selected grid number which has given satisfactory results for tripped airfoils.

3. Results and Discussion

3.1. Velocity vector plots

The flow structure over the airfoil with trip, for trip height of 0.7 mm at AOA of 4° for location 1 and 2 is shown in figures 7 and 8 respectively. The BLTs enhanced the boundary layer momentum exchange resulting in energized flow and elimination of the LSB. A recirculation region is observed just downstream the BLT, where the transition of the boundary layer from laminar to turbulent occurs as reported in [22]. The main aim of the study is to reduce such a dead air zone which is observed for the RT trip. The velocity vector plots show that IT trip introduces the longest recirculation region compared to the other two types for both the cases i.e, trip

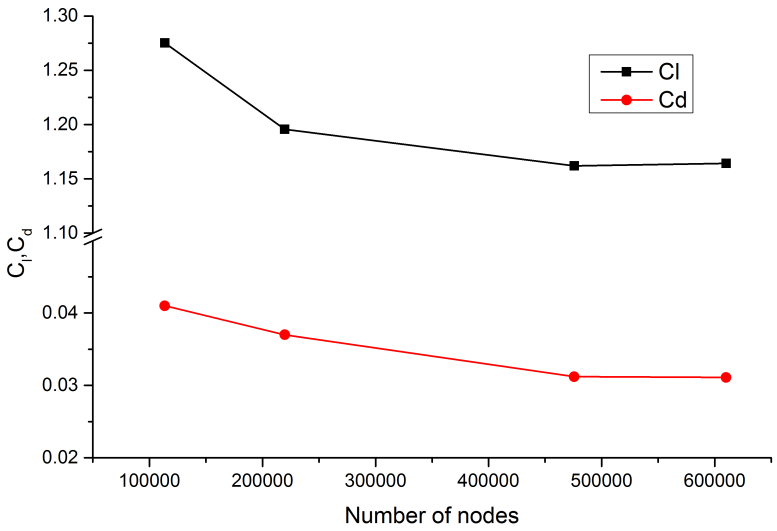

Figure 6: Effect of number of grid cells on lift and drag coefficient [22]

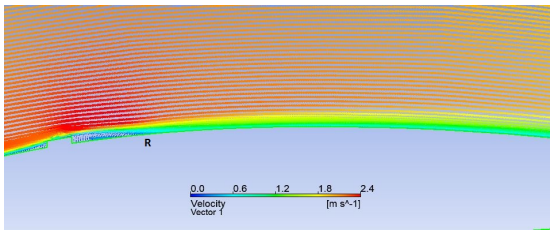

(a) RT trip [22]

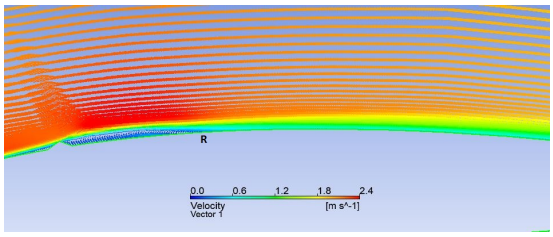

(b) IT trip

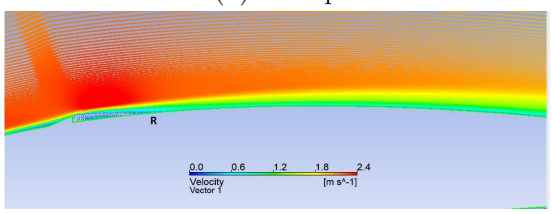

(c) RA trip

Figure 7: Velocity vector profile over the airfoil with trip height of 0.7 mm and at location-1 for AOA of 4° (R - flow re-attachment point)

at location-1 and location-2. But shortest recirculation (reattachment) length is observed for the RA trips. So from this particular perspective, the RA trip fulfils the required objective or shorter recirculation zone is created for the trip with a vertical rear face than that with slant

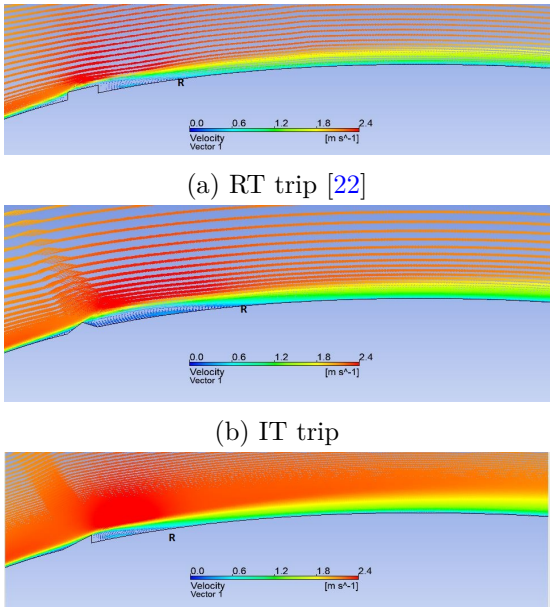

(a) RT trip [22]

(b) IT trip

(c) RA trip

Figure 8: Velocity vector profile over the airfoil with trip height of 0.7 mm and at location-2 for AOA of 4° (R - flow re-attachment point)

rear face. The LSB is eliminated by all three types of BLT at both the locations. Similar results are obtained with AOA of 6° and 8°.

3.2. C_p distribution

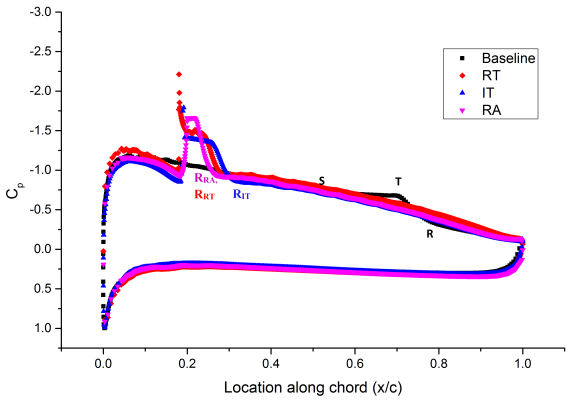

Figure 9: C_p distribution over the airfoil for trip height of 0.7 mm, location-1 and AOA of 4°

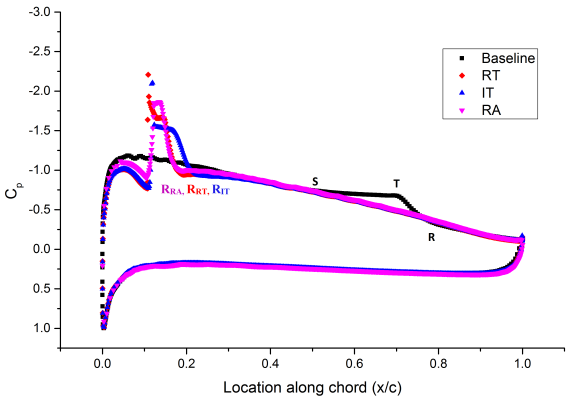

Figure 10: C_p distribution over the airfoil for trip height of 0.7 mm, location-2, and AOA of 4°

The Cp distribution over the airfoil surface with the IT and RA trip along with that on plain airfoil and airfoil with the RT trip (taken from [22]) is shown in figures 9 to 14. The Cp distribution is plotted in figures 9 and 10 for the trip height of 0.7 mm and AOA of 4° with trip located

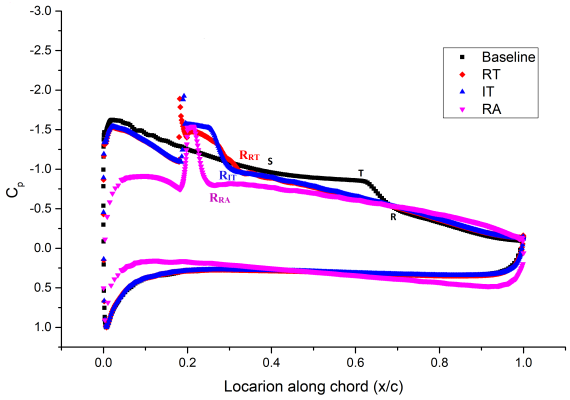

Figure 11: C_p distribution over the airfoil for trip height of 0.7 mm, location-1 and AOA of 6°

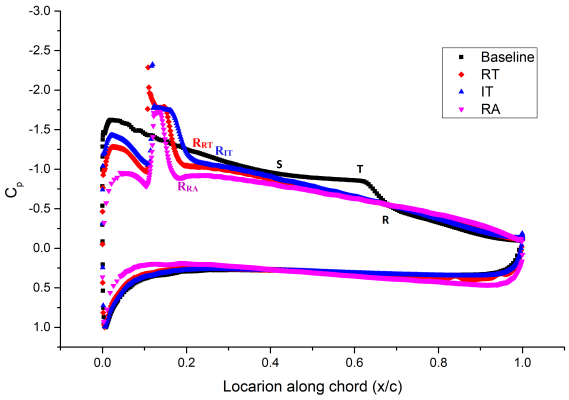

Figure 12: C_p distribution over the airfoil for trip height of 0.7 mm, location-2 and AOA of 6°

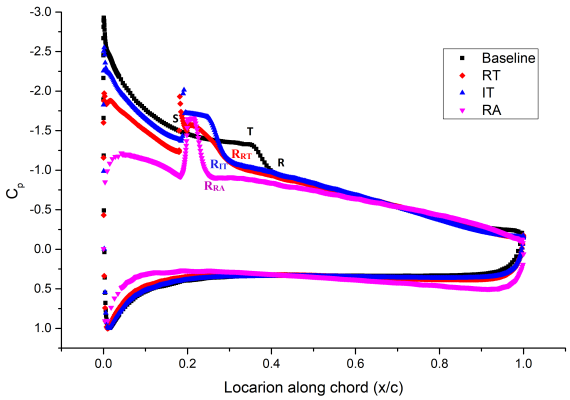

Figure 13: C_p distribution over the airfoil for trip height of 0.7 mm, location-1 and AOA of 8°

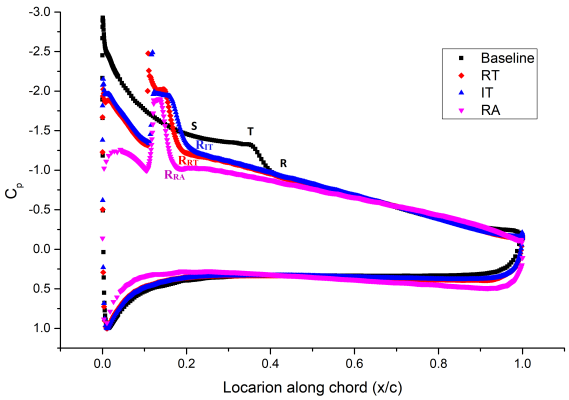

Figure 14: C_p distribution over the airfoil for trip height of 0.7 mm, location-2 and AOA of 8°

at location 1 and 2 respectively. The suction peak of all the tripped airfoils lies below that of the baseline airfoil. It may be concluded that the LSB is eliminated with the BLT as there is no observable pressure plateau on C_p distribution. A sudden jump in C_p on the suction surface of the airfoil, downstream the trip due to the flow obstruction caused by the trip, is observed for all three types of trips. This is evident from the vector plot also in the form of the recirculation region. The reattachment point of the boundary layer after the recirculation, for the RT and RA trip, is almost the same but the same for the IT is further down-stream. This is due to the geometrical peculiarity of the trip. Unlike the RA and RT, IT trip has an extended gradually declining surface after its maximum height. This surface makes the recirculating flow to attach gradually to airfoil surface resulting in an extended reattachment length. The C_p distribution for the airfoil with the RA trip is flatter than that for the airfoil with other two types of trips.

When the AOA increased to 6°, suction peak of tripped airfoil varies significantly. The suction peak is highest for the RA trip and lowest for the IT trip as shown in figures 11 and 12. The suction peak for baseline airfoil lies above that of the tripped airfoils. Complete elimination of

the LSB is achieved at this AOA as represented by smooth suction surface C_p distribution. At AOA of 8°, there is a large deviation in the magnitude of suction peak pressure for the tripped airfoil from baseline as well as from each other as shown in figures 13 and 14. When the AOA is 8°, the LSB moved upstream towards the leading edge for the baseline airfoil and is close to the BLT kept at location-1 (0.17c). This results in partial submerge of the BLT in the LSB as shown in figure 13.

3.3. Aerodynamic performance analysis

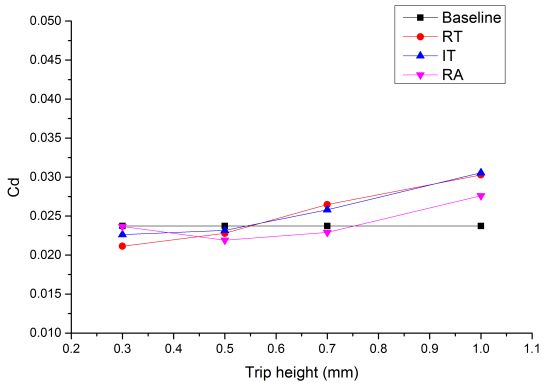

Figure 15: C_d v/s trip height for trip at location-1 and AOA of 4°

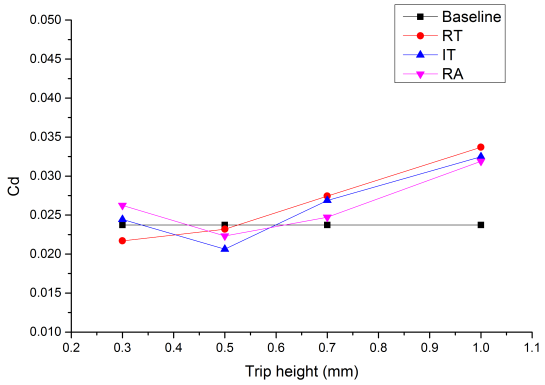

Figure 16: C_d v/s trip height for trip at location-2 and AOA of 4°

The effectiveness of the BLT can be examined by analysing the aerodynamic performance of the airfoil with and without the BLT. The total drag on a typical airfoil mainly consists of pressure drag and skin friction drag. An additional drag named bubble drag will be added when the LSB is formed on the airfoil surface. The purpose of providing BLT is to control the formation of the LSB and hence reduce the bubble drag. At the same time, the BLT will induce additional device drag due to the flow blockage and an additional skin friction drag due to the turbulent flow resulting from the forced transition of laminar flow to turbulent. To get a net reduction in total drag for the tripped airfoil, the increased drag due to BLT should be less than the reduction in bubble drag achieved by eliminating the LSB. In this section, the aerodynamic performance of the airfoil with the BLT is evaluated based on the net drag and the C_l/C_d ratio

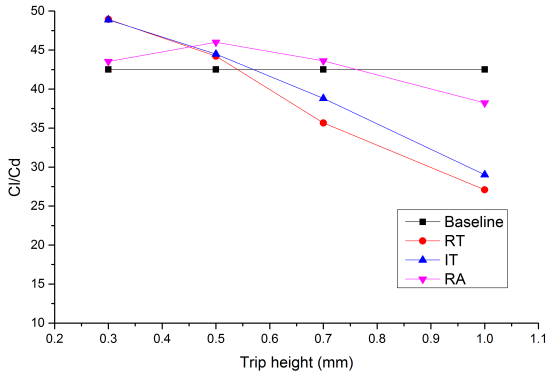

Figure 17: C_l/C_d v/s trip height for trip at location-1 and AOA of 4°

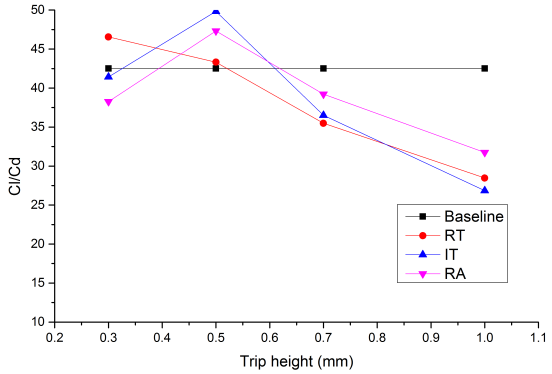

Figure 18: C_l/C_d v/s trip height for trip at location-2 and AOA of 4°

concerning that of the baseline airfoil.

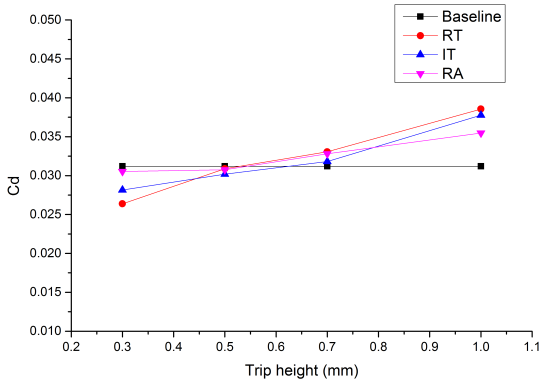

Figure 19: C_d v/s trip height for trip at location-1 and AOA of 6°

AOA 4° Figure 15 shows the variation of Cd with trip height for the baseline and tripped airfoils for the trip at location-1 (0.17c) at AOA of 4°. the tripped airfoils show better perfor-

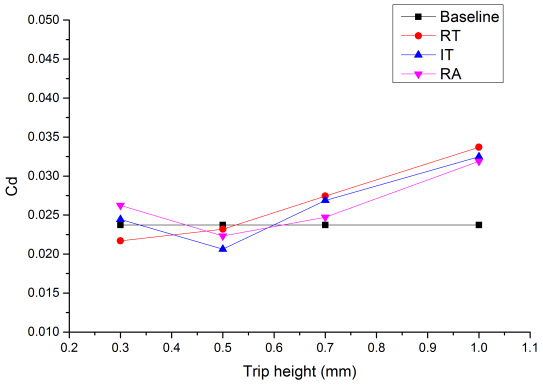

Figure 20: C_d v/s trip height for trip at location-2 and AOA of 6°

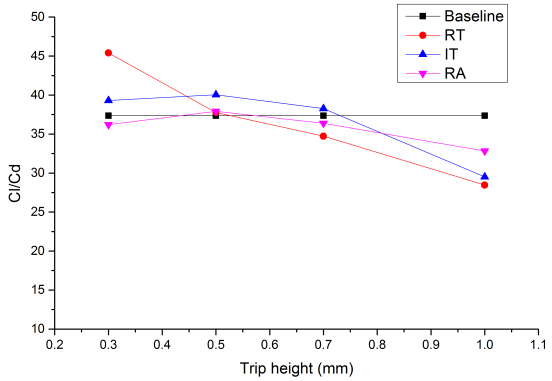

Figure 21: C_l/C_d v/s trip height for trip at location-1 and AOA of 6°

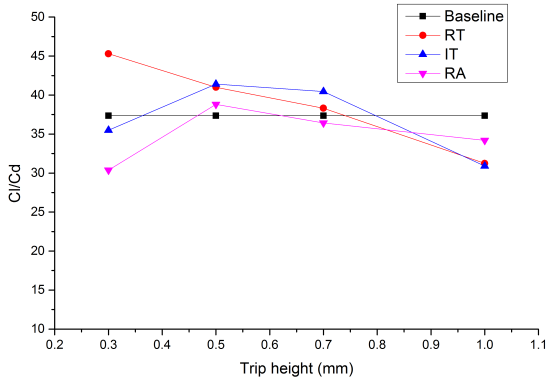

Figure 22: C_l/C_d v/s trip height for trip at location-2 and AOA of 6°

mance compared to baseline and the performance varies with trip height and shape. Different BTLs show improved performance at different trip heights. The RT BLT has the maximum advantage of 8.6% at the trip height of 0.3 mm at location-1 compared to the baseline and the performance is better than other types. As the trip height increases, the advantage gets reduced and beyond a height of 0.5 mm, the total drag coefficient becomes higher than that of the baseline. A similar trend is observed for the IT trip also with higher drag than that of the

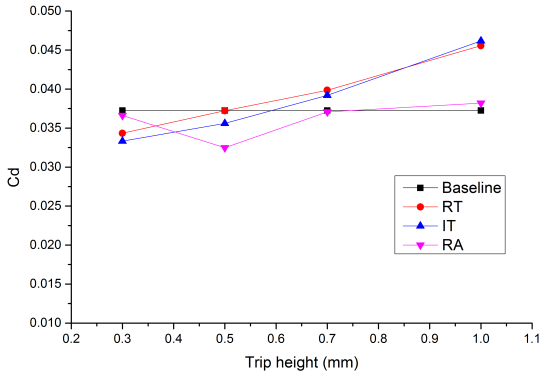

Figure 23: C_d v/s trip height for trip at location-1 and AOA of 8°

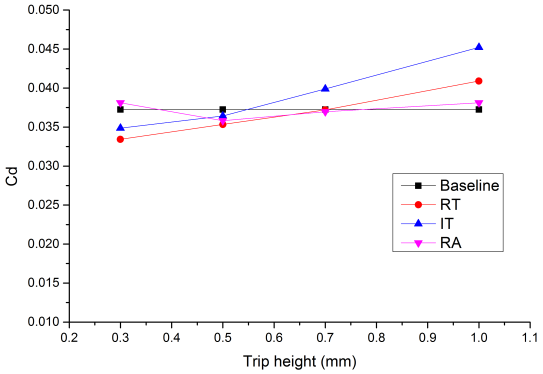

Figure 24: C_d v/s trip height for trip at location-2 and AOA of 8°

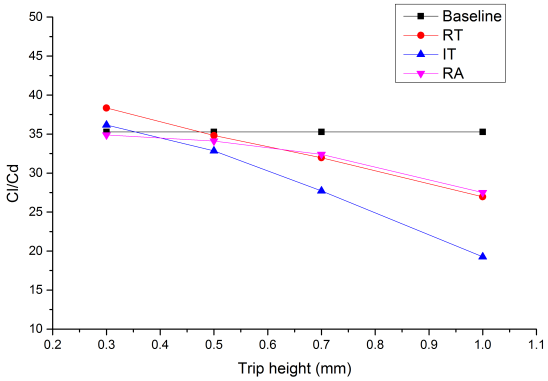

Figure 25: C_l/C_d v/s trip height for trip at location-1 and AOA of 8°

RT trip, but it is lower than that of the baseline till 0.5 mm trip height. For the RA trip, initial advantage on drag is very less and as the trip height increased it produced lower drag than that of the baseline till the trip height of 0.7 mm. The total drag is always lower than that for the RT and IT trips for trip height beyond 0.3 mm. As discussed previously, BLTs are effective only if the sum of the device drag and the additional skin friction drag due to turbulence is less than the bubble drag. It may be speculated that, up to the trip height of 0.5 mm, all three types

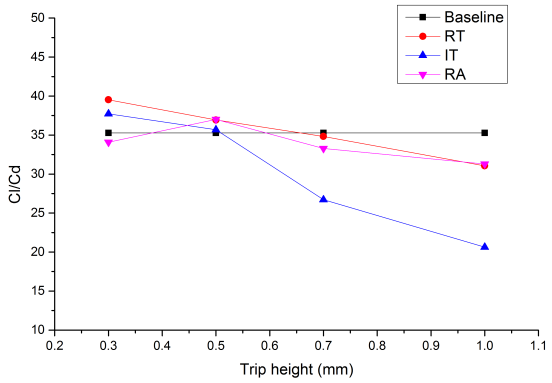

Figure 26: C_l/C_d v/s trip height for trip at location-2 and AOA of 8°

of trips promoted early flow transition and shortened the bubble. As the trip height increased, device drag also increased and resulted in higher total drag compared to baseline. For all the trip heights considered in the study, RT BLT produced the maximum device drag, because, its leading edge is normal to the flow whereas the leading edge is inclined in cse of the IT and RA trips. The blockage caused by the RA trip is minimum, and hence the total drag at higher trip heights is lower compared to the other two trips. Another important fact that can be observed from the plot is that the C_d value for the IT BLT is closer to that for the RT trip than that for the RA trip. This is due to two reasons - 1: increased device drag due to higher slope of the leading edge compared to RA trip, 2: increased frictional drag due to farther reattachment point (and longer recirculation region) of flow behind the trip due to the geometrical shape.

Similar performance is observed for all kind of trips when the trip is located at location-2. For 0.3 mm the trip height, both the IT and RA trips produce higher drag than that of baseline. For these trips at this height, the turbulence induced is insufficient to reduce bubble drag. Trip at location-1 shows better performance over that at location-2. The LSB is observed at a distance of 0.35c on baseline airfoil from leading edge at AOA of 4° [22]. The trip is location is fixed at a distance of 0.17c and 0.10c respectively from leading-edge for location-1 and 2. This means that the trip at location-2 is far upstream the LSB compared to trip in location-1, because of which the induced additional skin friction drag due to flow transition to turbulent is higher for the trip at location-2 compared to location-1.

Airfoil models with BLT at location-1 have better C_l/C_d value for both the RT trip and IT trip up to trip height of 0.5mm and for the RA trip up to 0.7 mm height as shown in figure 17. As the trip height increases, performance degraded due to the higher total drag. The total drag coefficient for RA trip is higher than that for other trips at 0.3 mm trip height and effect of the same is reflected with the least value in the C_l/C_d ratio. Also, the extended reattachment region with the IT trip at higher trip height affected the lift coefficient, and resulted in value of the C_l/C_d ratio closer to that for the RT BLT. When the trip is located at 0.10c, the RT trip has highest C_l/C_d ratio value of 47.56, which is higher by 11.9% of the baseline, but for other kind of trips, the value is lower than that for the baseline. But for the trip height of 0.5 mm, the IT and RA trips have higher C_l/C_d ratio than baseline and the RT trip. Beyond 0.5 mm height, all trips have lower C_l/C_d ratio than baseline.

AOA 6° Total drag coefficient of the airfoil with BLT at AOA 6° for location-1 is shown in figure 19. Up to trip height of 0.5 mm, all the BLTs produced lower drag than that for the baseline. The RT trip generates the least drag at the trip height of 0.3 mm, but with increase in trip height, the total drag coefficient of the RA trip becomes lesser than the other kind of trips. For the models with trip located at 0.10c (location-2), the RT trip performs better than the baseline till 0.7 mm trip height. The airfoil with other trip shapes performs better than the baseline for all the trip heights studied. The RA trip has superior performance over other models beyond the trip height of 0.7 mm due to its least resistance to flow. Reduction in net drag of the modified models results from the reduction of bubble drag which outweighs the induced device drag. As discussed previously, extended flow reattachment length of the IT trip results in long recirculation region and increase in the total drag of the model. Due to this reason, the total drag value of the model is closer to that for the RT trip. Trip at location-2 is far upstream from LSB than that at location-1(but the distance is lesser than that for AOA 4°). Hence, trip at location-2 induces sufficient turbulence than the trip at location-1. It resulted in elimination of LSB more effectively and produces lesser total drag than the trip at location-1.

Effect of trip on C_l/C_d ratio is presented in figures 21 and 22 . As in the case for the C_d, the RT trip is effective up to height of 0.5 mm for location-1 and up to 0.7 mm for location-2. The IT trip has slightly better ratio till 0.7 mm for location-1 than the baseline. For the same case with the trip at location-2, the advantage is restricted for trip heights between 0.5 mm to 0.7 mm. The RA trip has no advantage over the baseline for any of the cases. Except for trip height of 0.3 mm, in all other cases, providing trip at location-2 is advantageous.

AOA 8° At AOA of 8° also similar trend is observed as that in AOA 6° as shown in figures 23 and 24. The LSB moved upstream with increase in AOA. It resulted in reduced distance between the LSB and trip. It leads to slight increase in drag than that at AOA 6° compared to their corresponding baselines. The same reason holds good for the reduction in C_l/C_d ratio beyond the trip height of 0.7 mm compared to the baseline. The IT trip has lowest C_l/C_d ratio at higher trip heights, especially for location-1. The reason behind this is the longer reattachment of flow. The LSB is formed closer to the trip at location-1 and the separated flow attaches to the surface after the LSB formation.

3.4. Turbulent kinetic energy contour

This section illustrates the turbulent kinetic energy (TKE) distribution on the airfoil with and without BLT. Figure 27a shows the TKE distribution for baseline airfoil at AOA of 6°. High TKE is observed at a distance of 0.6c from leading-edge which represents the flow reattachment on the airfoil surface after the laminar separation. The flow is turbulent afterwards. The reattachment length after the trip aft reduces with increase in trip height as shown in figures 27b -27e where the contour is shown for the RA trip. From the figure, it can be seen that trip works as a vortex generator and the induced turbulence increases with trip height.

4. Conclusion

The effect of geometry (IT and RA), location and height of BLT on aerodynamic performance and LSB formation on E216 airfoil are numerically investigated using Transition $\gamma - Re_\theta$ turbulence model. The results are compared with that of the baseline and the RT trips from previous work of the authors [22]. In the majority of the cases of the airfoil with the BLT, because of additional turbulence, the LSB gets eliminated irrespective of the BLT shape. Different shapes

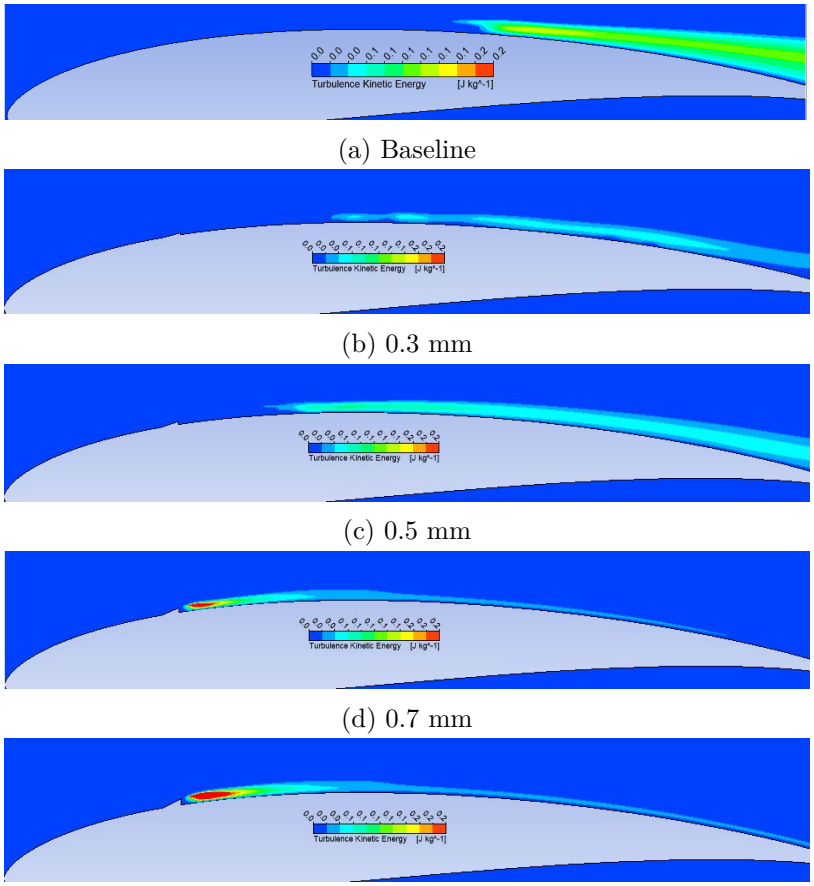

(a) Baseline

(b) 0.3 mm

(c) 0.5 mm

(d) 0.7 mm

(e) 1 mm

Figure 27: Distribution of TKE without (27a) and with BLT (27b - 27e) at AOA 6° and location-1 for RA trip

of BLT such as IT and RA have no specific advantage over the RT trip. In case of the RT trip, leading-edge is normal to the flow and hence it induced sufficient mixing even at lower trip heights (up to 0.5 mm) and hence shows better aerodynamic performance. For the other kind of trips, the leading edge is inclined to flow direction and hence the device drag is less but at the same time, the induced turbulence is also less at lower trip heights compared to the RT trip. The required mixing is achieved only at higher trip heights (beyond 0.3 mm). There exist an optimum trip height and location for each BLT at every AOA to achieve the optimum improvement in the aerodynamic performance of airfoil. Highest improvement in drag by 17.41% and corresponding lift to drag ratio by 10.86% are obtained for IT trip at location-2 for the angle of attack of 6° over the baseline.

As seen from the C_p plot, the presence of trip induces a jump in the surface pressure coefficient around the trip. To reduce the extent of this pressure jump, the thickness of the trip should be kept as minimum as possible. 3D studies are recommended for future work as the 2D assumption neglects the span-wise flow interactions. the LSB is purely a transient phenomenon and the present study is carried out with steady-state simulation. To completely understand the transitional behaviour of the LSB, transient simulation is recommended.

References

[1] Mathew S and Philip G S 2011 *Advances in wind energy and conversion technology* vol 20 (Springer)

[2] Clausen P and Wood D 1999 *Renewable Energy* **16** 922–927

[3] Standard I 2006 *International Electrotechnical Commission* **2**

[4] Lissaman P 1983 *Annual Review of Fluid Mechanics* **15** 223–239

[5] Sirignano W A 2013 *AIAA Journal* **51** 2045–2045

[6] Musial W and Cromack D 1988 *Journal of solar energy engineering* **110** 139–144

[7] Walker G 1992 The role of laminar-turbulent transition in gas turbine engines: a discussion *ASME 1992 International Gas Turbine and Aeroengine Congress and Exposition* (American Society of Mechanical Engineers) pp V001T01A108–V001T01A108

[8] Jahanmiri M 2011 Laminar separation bubble: its structure, dynamics and control Tech. rep. Chalmers University of Technology

[9] Jones B M 1934 *The Aeronautical Journal* **38** 753–770

[10] Selig M 2003 *VKI lecture series* 24–28

[11] Horton H P 1968 *Laminar separation bubbles in two and three dimensional incompressible flow.* Ph.D. thesis

[12] Singh R K and Ahmed M R 2013 *Renewable Energy* **50** 812–819

[13] Rist U and Augustin K 2006 *AIAA journal* **44** 2217

[14] Genc M S, Karasu I, Acikel H H, Akpolat M T and Genc M 2012 *Low Reynolds Number Aerodynamics and Transition, Genc, MS Ed.; InTech: Rijeka, Croatia* 1–28

[15] McCrossen T, Zakrzewski A and Pollock T 2010

[16] Bai T, Liu J, Zhang W and Zou Z 2014 *Propulsion and Power Research* **3** 82 – 89 ISSN 2212-540X URL http://www.sciencedirect.com/science/article/pii/S2212540X14000194

[17] Gopalarathnam A, Broughton B A, McGranahan B D and Selig M S 2003 *Journal of aircraft* **40** 768–775

[18] Jones A, Bakhtian N and Babinsky H 2008 *Journal of Aircraft* **45** 342–345

[19] Traub L W 2011 *Journal of Aircraft* **48** 1776–1784

[20] Simens M and Gungor A 2018 *European Journal of Mechanics-B/Fluids* **67** 70–78

[21] Lyon C A, Selig M S and Broeren A P 1997 *AIAA Paper* **511** 35

[22] Sreejith B and Sathyabhama A 2018 *Engineering science and technology, an international journal* **21** 77–88

[23] Medina H, Beechook A, Fadhila H, Aleksandrova S and Benjamin S 2018 *International Journal of Heat and Fluid Flow* **69** 150 – 163 ISSN 0142-727X URL https://www.sciencedirect.com/science/article/pii/S0142727X17306343

[24] Sreejith B and Sathyabhama A 2020 *Journal of the Brazilian Society of Mechanical Sciences and Engineering* **42** 1–15

[25] Crivellini A, D'Alessandro V, Di Benedetto D, Montelpare S and Ricci R 2014 Study of laminar separation bubble on low reynolds number operating airfoils: Rans modelling by means of an high-accuracy solver and experimental verification *Journal of Physics: Conference Series* vol 501 (IOP Publishing) p 012024

[26] Sheikholeslami M and Domiri Ganji D 2017 *Proceedings of the Institution of Mechanical Engineers, Part E: Journal of Process Mechanical Engineering* **231** 1235–1248

[27] Boudet J, Monier J F and Gao F 2015 *Journal of Thermal Science* **24** 30–36

[28] Sheikholeslami M and Ganji D 2016 *Energy Conversion and Management* **127** 112–123
[29] Dhawan S and Narasimha R 1958 *Journal of Fluid Mechanics* **3** 418–436
[30] Menter F R, Langtry R B, Likki S, Suzen Y, Huang P and Völker S 2006 *Journal of turbomachinery* **128** 413–422
[31] Menter F, Langtry R and Völker S 2006 *Flow, turbulence and combustion* **77** 277–303
[32] Langtry R B and Menter F R 2009 *AIAA journal* **47** 2894–2906
[33] FLUENT 2014 *Theory Guide*
[34] Shah H, Mathew S and Lim C M 2015 *International Journal of Energy and Environmental Engineering* **6** 419–429